Band-offset engineering in organic/inorganic semiconductor hybrid structures†

Sylke Blumstengel,* Hendrik Glowatzki, Sergey Sadofev, Norbert Koch, Stefan Kowarik, Jürgen P. Rabe and Fritz Henneberger

Received 6th April 2010, Accepted 30th June 2010
DOI: 10.1039/c004944c

Control over the electronic structure of organic/inorganic semiconductor interfaces is required to realize hybrid structures with tailored opto-electronic properties. An approach towards this goal is demonstrated for a layered hybrid system composed of *p*-sexiphenyl (6P) and ZnO. The molecular orientation can be switched from "upright-standing" to "flat-lying" by tuning the molecule–substrate interactions through aggregation on different crystal faces. The morphology change has profound consequences on the offsets between the molecular frontier energy levels and the semiconductor band edges. The combination of ZnO surface dipole modification through molecule adsorption and the orientation-dependence of the ionization energy of molecular layers shift these offsets by 0.7 eV. The implications for optimizing hybrid structures with regard to exciton and charge transfer are discussed.

1. Introduction

Adjustment of the energy levels at semiconductor hetero-interfaces is a key step for realizing aspired electronic and opto-electronic functions. In the present study, we address this issue for heterostructures made of inorganic and organic semiconductors. Such hybrid structures combine the complementary properties of conjugated organic materials (large absorption cross sections, high structural variability, function on the single-molecule level) and inorganic semiconductors (crystalline perfection, high charge carrier mobility, efficient electrical injection), promising thus substantial improvement of device performance or even entirely new functionalities. For our investigation, we have selected a planar geometry where an organic layer is deposited on top of an epitaxial inorganic film. This choice has the advantage of well-defined inter- and surfaces and, by this, electronic structure of the materials involved. Recently, non-radiative energy transfer between Wannier-Mott and molecular Frenkel excitons[1–3] as well as charge separation[4,5] have been observed for such layered hybrid systems for various material combinations.

The energies of interest are the valence band maximum (VBM) of the inorganic semiconductor and the position of the highest occupied molecular orbital (HOMO) as well as the minimum of the conduction band (CBM) and the position of the lowest unoccupied molecular orbital (LUMO). An obvious way to align these levels relative to each other might be searching for molecule-semiconductor pairs with appropriate energy spectrum. However, such search is made quite intricate by the fact that ionization potential and electron affinity of the isolated molecule can not be used as references, because these quantities are substantially modified by the specific intermolecular and molecule–substrate interactions occurring in contact with another material.[6] In what follows, we invert the problem and demonstrate that these interactions can be purposefully exploited for tuning the energy offsets in the hybrid structure. We are able to define different preferred orientations of a given molecular species on the same inorganic semiconductor by modifying the substrate-molecule interaction through deposition on different crystal faces. This enables us to tune the HOMO-VBM separation by 0.7 eV as a combined effect of surface dipole modification and the intramolecular dipole electrostatics in the molecular assemblies.

The molecule which allows for such a tuning is *p*-sexiphenyl (6P). 6P has an optical gap of about 3.1 eV, exhibits laser action under optical pumping,[7] and has been implemented in light-emitting diodes.[8] Due to its interesting optical properties, thin-film growth of 6P has been extensively investigated, both on metallic [Au(111), Al(111)] as well as dielectric surfaces (mica, TiO_2, KCl, GaAs).[9–11] For the inorganic semiconductor, we use ZnO because of its proven suitability of forming structurally well-defined hybrid structures with various conjugated organic molecules.[12] In addition, the 3.3 eV band-gap of ZnO matches well to 6P, thus furthering electronic coupling.

2. Experimental

The hybrid structures were grown under ultra-high vacuum conditions by molecular beam exitaxy (MBE) in a DCA 450 double-chamber MBE apparatus. In this way, the organic layer is deposited on a pristine and single-crystalline semiconductor surface to guarantee well-defined interfaces free of extrinsic defects. Organic materials were sublimed from Knudsen-type effusion cells with the deposition rate kept constant at 0.1 nm min^{-1} as measured by a quartz microbalance. The substrate temperature was varied between 290 and 450 K. ZnO is grown by radical-source MBE where atomic oxygen is provided by a RF plasma source (Addon),

Department of Physics, Humboldt University, 12489 Berlin, Germany. E-mail: sylke.blumstengel@physik.hu-berlin.de

† This paper contains work as a result of a collaborative research project of the German Science Foundation (DFG Sonderforschungsbereich 448) on "Mesoscopically organized composites"

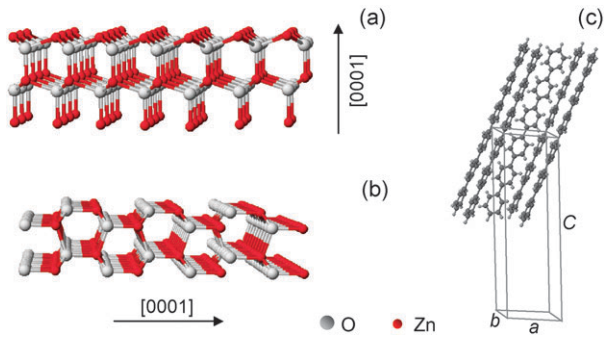

Fig. 1 Atomic structure of the (a) (0001) and (b) $(10\bar{1}0)$ ZnO surface. The lattice parameters of wutzite ZnO are $a = 3.253$ Å and $c = 5.211$ Å. (c) Unit cell of 6P projected on the (010) plane. The space group is $P2_1/c$ with lattice constants $a = 8.091$ Å, $b = 5.568$ Å, $c = 26.24$ Å and $\beta = 98.17°$.[14]

while the metal flux is produced by conventional effusion cells. We have selected the (0001) and $(10\bar{1}0)$ crystal face of the ZnO wurtzite structure in order to define different starting conditions for molecule aggregation. To obtain the desired film orientation, (0001) and $(10\bar{1}0)$ ZnO templates (Crystec) served as substrates. Substrate preparation and growth conditions are described in detail elsewhere.[13] The atomic structure of the surfaces is depicted in Fig. 1: The (0001) surface, oriented perpendicular to the polar *c*-axis, is terminated solely by Zn atoms, whereas the $(10\bar{1}0)$ surface contains the same number of Zn cations and O anions per unit area forming dimer rows with in-surface bonds along the *c*-axis.

The morphology of the 6P assemblage was analyzed by atomic force microscopy (AFM) measurements *ex-situ* in tapping mode (Nanoscope 3a, Veeco, USA). X-ray scattering measurements were conducted on an EFG X-ray diffractometer (Cu Kalpha radiation, Rigaku rotating anode X-ray generator, multi-layer Montel-optics) at a reduced background pressure of <10 mbar to protect the sample. Ultraviolet photoemission spectroscopy (UPS) using He I radiation (21.22 eV) and a Specs Phoibos 100 hemispherical energy analyzer was performed in order to unravel the electronic structure of the hybrid system. Secondary electron cutoff (SECO) spectra were obtained with the samples biased at -10 V in order to clear the analyzer work function. The experimental setup consisted of interconnected sample preparation (base pressure $<9 \times 10^{-9}$ mbar) and analysis (base pressure 1×10^{-10} mbar) chambers, which enabled sample transfer without breaking vacuum. Molecules were sublimed from resistively heated pinhole sources. The mass thickness of the organic layers was monitored with a quartz crystal microbalance. All experiments were carried out at room temperature.

3. Results

3.1 Morphology of 6P on different ZnO faces

Fig. 2 displays AFM images of the morphology of 6P on ZnO(0001). In the submonolayer regime (Fig. 2a and c), 6P islands of uniform height but without preferential in-plane orientation are visible. The height corresponds approximately to the length of the molecule, *i.e.*, the molecules stand nearly upright on the ZnO surface with the (001) plane as the contact plane. This morphology is found irrespective of the substrate temperature (290–450 K) during deposition. Whether the molecules assemble as in the equilibrium bulk structure (depicted in Fig. 1c) or in a surface-induced polymorph structure cannot be decided from AFM. However, all known polymorphs are layered herringbone structures. The fact that the molecules stand upright signifies that intermolecular interactions outbalance the molecule–substrate interaction. In the anisotropic herringbone crystals, the surface energy depends on the crystal faces and has a minimum for the 6P(001) plane. Due to the hexagonal symmetry of the ZnO surface, no single preferential in-plane orientation of the 6P crystallites is expected. The mean island size as well as the mean distance between the islands increase with increasing substrate temperature for a given deposition rate, which is typical for a diffusion-mediated growth process, as found for 6T on ZnO(0001).[15] Continuing the deposition, the growth direction is retained resulting in terraced islands with step heights corresponding to almost the length of the 6P molecule (see Fig. 2d). At low substrate temperature (290 K), rod-like crystallites are additionally present indicating the formation of a secondary orientation at an advanced growth stage (Fig. 2b).

The situation is profoundly changed for aggregation on ZnO$(10\bar{1}0)$. For deposition at room temperature and in the submonolayer regime, needle-shaped nuclei are visible besides the islands comprising upright standing molecules (Fig. 3a). Upon further deposition of 6P, the needles grow and eventually coalesce (Fig. 3b). At higher substrate temperatures (373 K), 6P aggregates already in the initial stage exclusively in crystalline needles (Fig. 3c) with a uniform height of about 10 nm (Fig. 3d). Such a morphology is formed, when the molecules adsorb flat-lying, *i.e.*, with their long axis (approximately) parallel to the substrate surface. Subsequent aggregation and crystal formation is then determined by the anisotropy of the growth velocity in the herringbone structure which is slower in [001] direction compared to [100] and [010]. In order to actuate flat-lying adsorption, the molecule–substrate interaction must be markedly stronger than on ZnO(0001). Needle-shaped 6P aggregation has been found also on other substrates like mica, KCl(100) and oxygen-reconstructed TiO_2(110) and various contact planes of the 6P crystal have been identified.[9] In the present case, the needles are well aligned with their axis parallel to the ZnO *c*-axis. X-ray diffraction (not shown) performed on the 6P layer depicted in Fig. 3b yields that the 6P$(20\bar{3})$ crystal plane is the contact plane. Consequently, the molecules lie perfectly flat on the ZnO surface with their long axis parallel to the alternating rows of oxygen and zinc (Fig. 1b). This is in agreement with measurements of the 6P photoluminescence polarization (not shown), indicating also that the molecules are orientated at an angle of 90° with respect to the needle axis.

We have also investigated the assemblage of 6P on the O-terminated $(000\bar{1})$ ZnO surface. Here, "flat-lying" and "upright-standing" morphologies occur side-by-side irrespective of the growth temperature. All these findings underline the critical role of the semiconductor surface, both in terms of

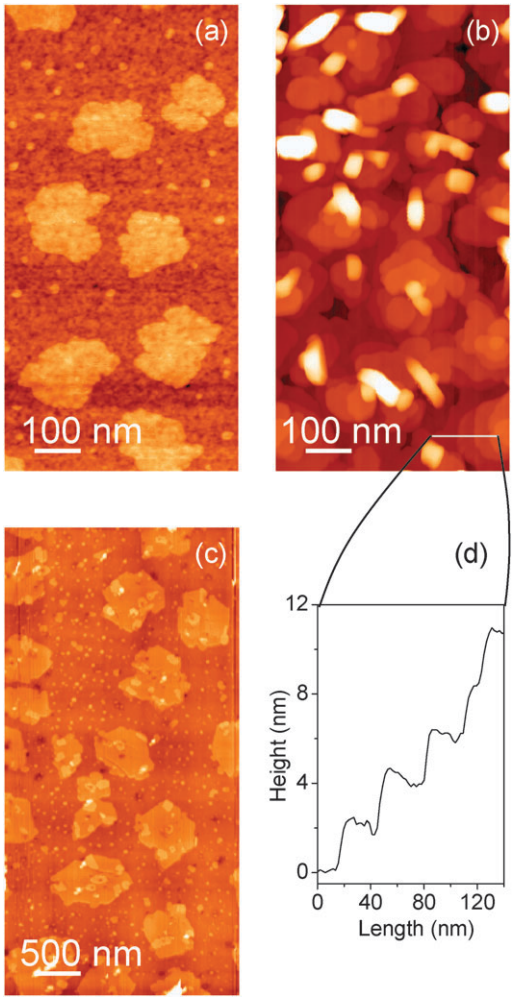

Fig. 2 AFM images of 6P on ZnO(0001) for a nominal thickness of 1 nm (a),(c) and 12 nm (b). The substrate was kept during 6P deposition at 293 K (a),(b) and 373 K (c). The hight profile (d) is taken along the line in image (b).

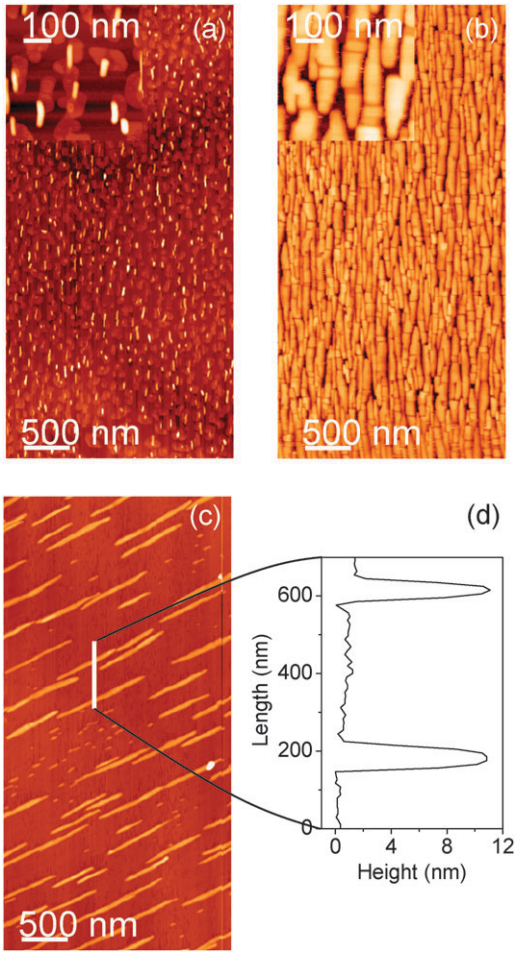

Fig. 3 AFM image of 6P on ZnO(10$\bar{1}$0) for a nominal thickness of 1 nm (a) and (c) and 12 nm (b). During 6P deposition, the substrate was kept at 293 K (a), (b) and 373 K (c). The hight profile (d) is taken along the line in image (c).

atomistic structure as well as growth kinetics, for the type of molecular aggregation.

3.2 Electronic structure of 6P/ZnO interfaces

UPS spectra of the 6P/ZnO(0001) and 6P/ZnO(10$\bar{1}$0) hybrid systems are summarized in Fig. 4a and b, respectively. The valence spectra of pristine ZnO in the energy range from 3 to 9 eV (upper curves in right panels) are characteristic of the specific surface. For ZnO(0001), the spectrum is dominated by the O 2*p*-Zn 4*sp* valence band states,[16,17] while a second feature at 3.7 eV present for ZnO(10$\bar{1}$0) originates from the O 2p dangling bond state.[16] The VBM binding energies taken from the emission onsets are 3.15 eV and 2.90 eV, respectively. Upon deposition of 6P, the emissions due to molecular levels of 6P become increasingly apparent, particularly those of the HOMO and HOMO-1. Their intensity ratio reflects the molecular orientation with respect to the surface due to UPS selection rules in the experimental geometry used. For the 6P/ZnO(0001) hybrid structure, these features emerge at binding energies of 2.50 eV and 3.00 eV, respectively. No appreciable energy shift is observed with increasing 6P deposition up to a mass thickness of d_{6P} = 6 nm signifying that bend banding plays no essential role. The intensity ratio of HOMO and HOMO-1, also thickness independent, is that of upright standing molecules, consistent with the morphology revealed by AFM. This also rules out the presence of a wetting layer composed of flat-lying molecules as observed in 6P films grown on TiO_2(110).[11] The work function derived from the SECO (Fig. 4a, left) of pristine ZnO(0001) is ϕ = 3.85 eV. Deposition of 6P lowers ϕ by 0.20 eV. This reduction is observed already at lowest coverage and remains constant throughout further deposition of 6P. The ionization potential, measured as the difference between the HOMO onset and the vacuum level (VL), amounts to 5.65 eV.

Marked differences are observed for the 6P/ZnO(10$\bar{1}$0) hybrid interface. First, HOMO and HOMO-1 emissions (Fig. 4b, right) are now located at binding energies of 2.90 eV and 3.40 eV, respectively, *i.e.*, shifted to higher binding energy by 0.40 eV with respect to the ''upright-standing'' case on the ZnO(0001) surface. Second, the intensity ratio of HOMO and HOMO-1 is *ca.* 1 : 1, indicating flat-lying molecules, again in agreement with the AFM and XRD data. Third, the work function is changed significantly (Fig. 4b, left). It decreases

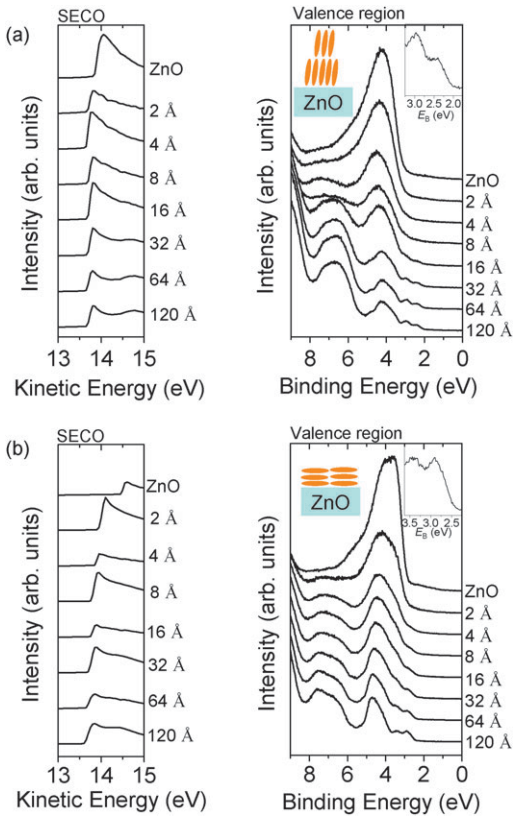

Fig. 4 SECO and valence region UPS spectra of 6P on ZnO(0001) (a) and ZnO(10$\bar{1}$0) (b) for increasing mass thickness of the organic layer. The inset left schematises the molecular orientation on the ZnO surface, while the inset right is a blow-up of the HOMO and HOMO-1 region of the UPS spectrum for 6P layer thickness of 120 Å.

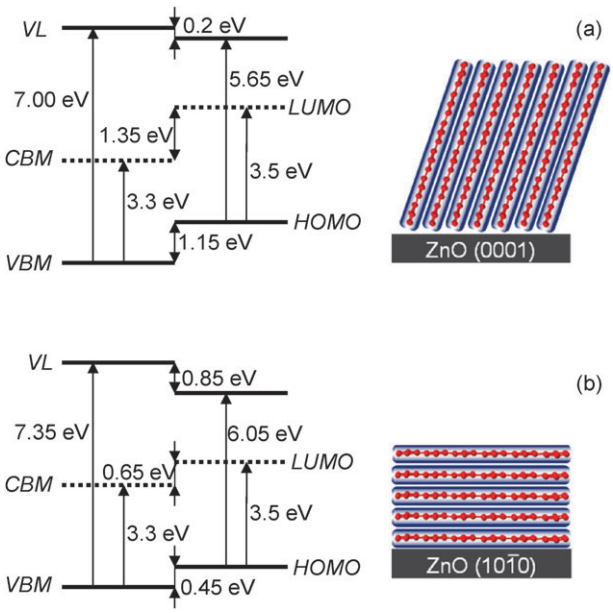

Fig. 5 Energy level alignment at the 6P/ZnO (0001) (a) and 6P/ZnO(10$\bar{1}$0) (b) interfaces derived from UPS and optical absorption data taking into account the respective exciton binding energies (see text). Energy values are rounded. The panels on the right side show the molecular orientation on ZnO as well as the distribution of the charges in the layers to visualize the origin of the orientation-dependent ionization potential. Red: positively charged molecular backbone, blue: negatively charged π-electron cloud.

from ϕ = 4.45 eV for the pristine ZnO(10$\bar{1}$0) surface down to ϕ = 3.60 eV. The major part of this shift is already established at lowest coverage, while a smaller contribution evolves still gradually with increasing mass thickness. The latter is not related to a work function change induced by multilayer formation because 6P has no intrinsic molecular dipole. Instead, this observation is a consequence of the 6P growth mode, where needle-shaped multilayer islands form before the 6P monolayer is fully completed. This means that even for comparably high nominal 6P mass thickness there are still uncovered ZnO patches, and the local work function for pristine ZnO and 6P-covered ZnO is different. Since the measured work function is an area-weighted average, its value changes as function of coverage until the 6P monolayer is fully closed. Homogenous energy levels in 6P are confirmed by constant HOMO and HOMO-1 binding energies and intensity ratio, as well as the absence of notable spectral broadening. The ionization potential of flat-lying 6P amounts to 6.04 eV, *i.e.*, is increased by 0.4 eV with respect to the "upright standing" morphology.

4. Discussion and conclusions

The energy level diagrams of the two different 6P/ZnO hybrid structures derived from the UPS measurements are represented in Fig. 5. The CBM and LUMO positions of ZnO and 6P are estimated using band-gap energies obtained from absorption data corrected by the exciton binding energies of 0.06 eV and 0.4 eV,[18] respectively.

The different work functions of the pristine ZnO films are related to their different surface dipole moments. In both cases, adsorption of 6P lowers the work function and thus the VL, as has been commonly observed for organic layers grown on metals and ZnSe.[19–21] In the absence of strong chemical interaction between molecules and metals, the work function reduction is explained by the "push-back" effect,[19,20] where the metal surface dipole is reduced by molecule adsorption due to Pauli-repulsion. Since 6P and ZnO also exhibit rather weak interaction, we suggest that Pauli-repulsion and the associated charge redistribution may be the dominating effect for the observed work function reduction. A detailed understanding of these interfaces, however, will still require considerable experimental and theoretical investigations. Interestingly, the work function reduction of ZnO(10$\bar{1}$0) with the initially larger ϕ is stronger so that the work function of both hybrid structures is finally quite similar. The more pronounced charge redistribution at the (10$\bar{1}$0) interface is consistent with a stronger molecule/substrate interaction needed to establish a "flat-lying" molecular orientation. If this interaction becomes too strong, the molecular structure may be destroyed or the conjugation disturbed. The presence of clear valence features without differential shifts in the UPS spectra indicate that 6P adsorbs chemically intact also on the stronger interacting (10$\bar{1}$0) surface. Needle growth along the polar *c*-axis and molecular alignment perpendicular to it indicate that also in-plane dipoles play a role in the molecular

aggregation at this surface. Note that the absence of band bending in both hybrid structures rules out noticeable charge transfer between the inorganic and organic component.

A further prominent finding is that the ionization energy of the molecules in the "flat-lying" morphology is by 0.4 eV higher as compared to the "upright-standing" case, translating in an additional low-energy shift of the 6P HOMO towards the ZnO VBM. The reason of this shift is the collective electrostatics of intra-molecular polar bonds[22,23] in the differently ordered molecular structures (see right panels Fig. 5). In the "flat-lying" orientation, the π-electron system is orientated parallel to the surface forming thus a negatively charged plane which increases the energy barrier for electron release. In contrast, charge neutrality (or slight positive charges due to terminal hydrogens) is characteristic of the "upright-standing" morphology. The ZnO surface is required to induce the particular type of aggregation, however, the energy difference is solely a feature of the molecular system.

The combination of both effects – surface-dipole modification and orientation-dependent electrostatics – provides an overall shift of the VBM-HOMO offset of 0.7 eV between the two different hybrid structures. This finding has immediate consequences for the opto-electronic function of hybrid structures. When aiming at electron injection from the inorganic semiconductor, the charge injection barrier can be substantially reduced by using the appropriate interface. The exact behavior of CBM and LUMO energies require extra investigation. The estimate based on the transport band-gaps of the separate materials provides a type-II alignment, *i.e.*, VBM-HOMO and CBM-LUMO offset have the same sign. Such an alignment facilitates exciton dissociation at the interface as a basic step for photovoltaic applications. In the present hybrid structures, the energy gain of 0.65–1.35 eV by separating electron (ZnO) and hole (6P) exceeds markedly the exciton binding energy so that this process is indeed prevailing. On the other hand, if one aims at hybrid light-emitting devices utilizing electrical injection *via* the inorganic part, type-II energy alignment is not favorable. The ZnO band-gap can be enlarged through incorporation of Mg by about 1 eV.[24] Previous studies of SP6 on ZnO and ZnMgO have demonstrated that the VBM-HOMO offset remains nearly constant so that the band-gap widening transforms mostly in a respective decrease of the CBM-LUMO separation.[4] In this way, one should be able to block first exciton dissociation and, eventually, to arrive at a true type-I alignment with the VBM-HOMO offset negative and CBM-LUMO offset positive. The morphology of the molecular assemblage is also essential for the efficiency of non-radiative Förster-type energy transfer. The orientation – flat-lying or upright-standing – defines the direction of the optical dipole moment. Therefore, depending on the dipole moment of the inorganic exciton, this transfer can be maximal or made to disappear.

In this work, we have demonstrated that the molecular orientation in organic films can be switched by using different crystal faces of a given inorganic semiconductor. An interesting next step will be to control the molecular orientation for one and the same semiconductor surface. A strategy that might allow for achieving this goal is organic growth on vicinal semiconductor surfaces where well-defined step edges will be exploited to tune the molecule-substrate interaction.

Acknowledgements

The authors acknowledge financial support by DFG *via* Sfb 448.

References

1 S. Blumstengel, S. Sadofev, C. Xu, J. Puls and F. Henneberger, *Phys. Rev. Lett.*, 2006, **97**, 237401.
2 G. Itskos, G. Heliotis, P. G. Lagoudakis, J. Lupton, N. P. Barradas, E. Alves, S. Pereira, I. M. Watson, M. D. Dawson, J. Feldmann, R. Murray and D. D. C. Bradley, *Phys. Rev. B: Condens. Matter Mater. Phys.*, 2007, **76**, 035344.
3 S. Chanyawadee, P. G. Lagoudakis, R. T. Harley, D. G. Lidzey and M. Henini, *Phys. Rev. B: Condens. Matter Mater. Phys.*, 2008, **77**, 193402.
4 S. Blumstengel, S. Sadofev, C. Xu, J. Puls, R. L. Johnson, H. Glowatzki, N. Koch and F. Henneberger, *Phys. Rev. B: Condens. Matter Mater. Phys.*, 2008, **77**, 085323.
5 H. Kim, Q. Zhang, Y.-K. Song, A. Nurmikko, Q. Sun and J. Han, *Phys. Status Solidi C*, 2009, **6**, 593.
6 N. Ueno and S. Kera, *Prog. Surf. Sci.*, 2008, **83**, 490.
7 F. Quochi, F. Cordella, A. Mura, G. Bongiovanni, F. Balzer and H.-G. Rubahn, *Appl. Phys. Lett.*, 2006, **88**, 041106.
8 F. Meghdadi, S. Tasch, B. Winkler, W. Fischer, F. Stelzer and G. Leising, *Synth. Met.*, 1997, **85**, 1441.
9 R. Resel, *J. Phys.: Condens. Matter*, 2008, **20**, 184009.
10 K. Erlacher, R. Resel, S. Hampel, T. Kuhlmann, K. Lischka, B. Muller, A. Thierry, B. Lotz and G. Leising, *Surf. Sci.*, 1999, **437**, 191.
11 L. Sun, S. Berkebile, G. Weidlinger, G. Koller, M. Hohage, F. P. Netzer, M. G. Ramsey and P. Zeppenfeld, *Phys. Chem. Chem. Phys.*, 2010, **12**, 3141.
12 S. Blumstengel, S. Sadofev and F. Henneberger, *New J. Phys.*, 2008, **10**, 065010.
13 S. Sadofev, P. Schäfer, Y.-H. Fan, S. Blumstengel, F. Henneberger, D. Schulz and D. Klimm, *Appl. Phys. Lett.*, 2007, **91**, 201923.
14 K. N. Baker, A. V. Fratini, T. Resch, H. C. Knachel, W. Adams, E. Socci and B. Farmer, *Polymer*, 1993, **34**, 1571.
15 S. Blumstengel, N. Koch, S. Sadofev, P. Schäfer, H. Glowatzki, R. L. Johnson, J. P. Rabe and F. Henneberger, *Appl. Phys. Lett.*, 2008, **92**, 193303.
16 K. Ozawa, K. Sawada, Y. Shirotori, K. Edamoto and M. Nakatake, *Phys. Rev. B: Condens. Matter Mater. Phys.*, 2003, **68**, 125417.
17 R. T. Girard, O. Tjernberg, G. Chiaia, S. Söderholm, U. O. Karlsson, C. Wigren, H. Nylén and I. Lindau, *Surf. Sci.*, 1997, **373**, 409.
18 P. Puschnig and C. Ambrosch-Draxl, *Monatsh. Chem.*, 2008, **139**, 389.
19 H. Ishii, K. Sugiyama, E. Ito and K. Seki, *Adv. Mater.*, 1999, **11**, 605.
20 A. Kahn, N. Koch and W. Gao, *J. Polym. Sci., Part B: Polym. Phys.*, 2003, **41**, 2529.
21 S. Blumstengel, N. Koch, S. Duhm, H. Glowatzki, R. Johnson, C. Xu, A. Yassar, J. Rabe and F. Henneberger, *Phys. Rev. B: Condens. Matter Mater. Phys.*, 2006, **73**, 165323.
22 S. Duhm, I. Salzmann, N. Koch, H. Fukagawa, T. Kataoka, S. Hosoumi, K. Nebashi, S. Kera and N. Ueno, *J. Appl. Phys.*, 2008, **104**, 033717.
23 S. Duhm, G. Heimel, I. Salzmann, H. Glowatzki, R. Johnson, A. Vollmer, J. P. Rabe and N. Koch, *Nat. Mater.*, 2008, **7**, 326.
24 S. Sadofev, S. Blumstengel, J. Cui, J. Puls, S. Rogaschewski, P. Schäfer, Y. G. Sadofyev and F. Henneberger, *Appl. Phys. Lett.*, 2005, **87**, 091903.

